Self-consistent gauge-invariant theory of the in-plane infrared response of high-T_c cuprate superconductors

Jiří Chaloupka* and Dominik Munzar
Department of Condensed Matter Physics, Faculty of Science, Masaryk University, Kotlářská 2, 61137 Brno, Czech Republic
(Received 14 August 2007; published 4 December 2007)

We report on results of our theoretical study of the in-plane infrared conductivity of the high-T_c cuprate superconductors using the model where charged planar quasiparticles are coupled to spin fluctuations. The computations include both the renormalization of the quasiparticles and the corresponding modification of the current-current vertex function (vertex correction), which ensures gauge invariance of the theory and local charge conservation in the system. The incorporation of the vertex corrections leads to an increase of the total intraband optical spectral weight (SW) at finite frequencies, a SW transfer from far infrared to mid infrared, a significant reduction of the SW of the superconducting condensate, and an amplification of characteristic features in the superconducting state spectra of the inverse scattering rate $1/\tau$. We also discuss the role of self-consistency and propose an interpretation of a kink occurring in the experimental low temperature spectra of $1/\tau$ around 1000 cm^{-1}.

DOI: 10.1103/PhysRevB.76.214502 PACS number(s): 74.25.Gz, 74.72.−h

I. INTRODUCTION

Most of the existing calculations of the frequency dependent conductivity σ in high-T_c cuprate superconductors (for representative examples, see Refs. 1–7) employ the approximation where interactions of the excited states are not taken into account, i.e., the so-called vertex corrections (VCs) in the perturbation expansion for σ are neglected. It is well known that this approach is not gauge invariant, and the results may depend on the gauge of the vector and scalar potentials. Physically, gauge-invariant response is a manifestation of local charge conservation in the system. We recall that the usual restricted conductivity sum rule for the normal state (NS)

$$I_f = -(\pi e^2/2\hbar^2)K, \tag{1}$$

where

$$I_f = \int_{0^+}^{\infty} \sigma_{1x}(\omega) d\omega \tag{2}$$

is the intraband optical spectral weight and

$$K = -\frac{1}{V}\sum_{k\alpha} \frac{\partial^2 \varepsilon_k}{\partial k_x^2} n_{k\alpha}, \tag{3}$$

the so-called effective kinetic energy per unit cell (α stands for the spin index, ε_k is the dispersion relation, and $n_{k\alpha}$ is the occupation factor), is a consequence of the gauge invariance.[8] For concreteness, we have considered the conductivity along the x axis. The NS conductivity calculated using a no-VC approach thus need not satisfy the sum rule. Similarly, for the superconducting state (SCS), the spectral weight of the condensate I_c, which is given by

$$I_f + I_c = -(\pi e^2/2\hbar^2)K, \tag{4}$$

as obtained within a no-VC calculation, may be rather different from that of the corresponding gauge-invariant approach. These possible problems call for an assessment of the contribution of the relevant VC to I_f.

Another reason for studying the VC has been highlighted by Millis and coworkers. If the VC were negligible, the infrared (IR) conductivity would be determined solely by the quasiparticle self-energy that can be, at least in principle, extracted from photoemission data. Millis and Drew[9] found out, however, that the effective scattering rate in optimally doped $Bi_2Sr_2CaCu_2O_{8+\delta}$, obtained using the self-energy estimated from the photoemission data, is much higher than the value resulting from the IR data. Similarly, Millis *et al.*[10] demonstrated that the local self-energy obtained by fitting (without VC) the IR data of thin films of $Pr_{2-x}Ce_xCuO_{4+\delta}$ leads to much lower (by a factor of 3–4) values of the quasiparticle velocity than observed by photoemission. These discrepancies appear to imply the presence of a large VC.

A brief account of the VC to the NS conductivity of cuprate superconductors has been given by Monthoux and Pines in one of the pioneering papers on the nearly antiferromagnetic Fermi liquid model.[11] For this particular model, the VCs have been found to cause a slight increase (about 20%) of resistivity. Current vertex renormalization within the conserving fluctuation exchange approach[12] has been systematically investigated by Kontani (see, e.g., Refs. 13 and 14, and references therein). He successfully explained the anomalous temperature dependence of the Hall conductivity in cuprates and estimated the contribution of the VC to the normal state conductivity. Benfatto *et al.*[15] and Aristov and Zeyher[16] discussed the role of the VC in the context of optical response of systems possessing the d-density wave ground state that might occur in the pseudogap regime of underdoped cuprates. We are not aware, however, of any work incorporating the VC in computations of the optical response in the superconducting state.

The purpose of the present study is to explore the role played by the VC, both in the NS and in the SCS, within the spin-fermion model, where charged planar quasiparticles are coupled to spin fluctuations (SFs). We discuss the violation, in the absence of VC, of the NS sum rule and the impact of the VC on the dc conductivity, on the spectral weight of the superconducting condensate, and on the shape of $\sigma_1(\omega)$. An

important finding is that the incorporation of the VC leads to a spectral-weight shift from far infrared (FIR) to midinfrared (MIR). Finally, we address the related changes of sharp structures in the inverse scattering rate $[1/\tau](\omega)$.

The rest of the paper is organized as follows. In Sec. II, we present the basic equations of the theory, the values of the input parameters, and some computational details. Since part of the formalism has been already detailed in the related previous work by Cásek *et al.*,[6] we keep the account short. Section III contains our results and discussion. The quasiparticle Green's functions have been obtained here using a fully self-consistent Eliashberg theory, whereas an approximate non-self-consistent approach, where the BCS propagator is corrected by the coupling to the SF, has been adopted in Ref. 6. In order to clarify the role of self-consistency, we first neglect the VC and compare the results of the two approaches (Sec. III A). In Sec. III B, we then focus on the contribution of the vertex corrections. The summary and conclusions are given in Sec. IV.

II. THEORY, INPUT PARAMETERS, AND COMPUTATIONAL DETAILS

Within the framework of the spin-fermion model, the electronic quasiparticles are renormalized via a coupling to SF. These are described by the spin susceptibility $\chi_{\mathrm{SF}}(\boldsymbol{k},E)$ of the form motivated by neutron data, and the electronic self-energy (2×2 matrix) of the most sophisticated version of the theory is given by[17]

$$\Sigma(\boldsymbol{k},iE)=\frac{g^2}{\beta N}\sum_{\boldsymbol{k}',iE'}\chi_{\mathrm{SF}}(\boldsymbol{k}-\boldsymbol{k}',iE-iE')\mathcal{G}(\boldsymbol{k}',iE'). \quad (5)$$

Here, g is the coupling constant, χ_{SF} is the Matsubara counterpart of the spin susceptibility, and $\mathcal{G}$ is the Nambu propagator of the renormalized electronic quasiparticles, $\mathcal{G}=[iE\tau_0-(\epsilon_{\boldsymbol{k}}-\mu)\tau_3-\Sigma(\boldsymbol{k},iE)]^{-1}$. The sum runs through the Bloch vectors $\boldsymbol{k}'$ in the first Brillouin zone (N in total) and the fermionic Matsubara energies $iE'=i\pi(2n+1)/\beta$. Note that Eq. (5) is a compressed form of the generalized Eliashberg equations. In contrast to the standard Eliashberg equations as described, e.g., in Ref. 20, the equation involves the full momentum dependence of the self-energy and it does not involve any approximation regarding the density of states and any factorization of the momentum integral. Note, further, that the theory does not include any vertex corrections in the self-energy diagram.

A popular approximation to the fully self-consistent treatment of Eq. (5), used, e.g., in Refs. 1, 6, and 18, consists in starting with the BCS Nambu propagator with an estimated superconducting gap of $d_{x^2-y^2}$ symmetry and including the lowest order correction due to the coupling to the SF. If we write the right hand side of Eq. (5) as a convolution, $\Sigma=g^2\chi_{\mathrm{SF}}\star\mathcal{G}$, then the latter approach, called the hybrid approach in the following, yields $\Sigma_h=\Delta_{\boldsymbol{k}}\tau_1+g^2\chi_{\mathrm{SF}}\star\mathcal{G}_0$, where $\mathcal{G}_0$ stands for the BCS propagator with the gap $\Delta_{\boldsymbol{k}}$. This description is particularly suitable for situations where the coupling to the SF is not the only cause of superconductivity, and provides an *additional* renormalization of the quasiparticles. The magnitude of the superconducting gap can be tuned by changing the input amplitude Δ_0 of $\Delta_{\boldsymbol{k}}$. An important advantage of the hybrid approach is that it avoids the necessity of numerical continuation from Matsubara frequencies to the real axis.

Within the framework of the linear response theory, the optical conductivity is given by the Kubo formula

$$\sigma_{ij}(\boldsymbol{q},\omega)=\frac{(e^2/\hbar^2)K_{ij}+\Pi_{ij}(\boldsymbol{q},\omega)}{i(\omega+i\delta)}, \quad (6)$$

where K_{ij} is the diamagnetic tensor,

$$K_{ij}=-\frac{1}{V}\sum_{\boldsymbol{k}\alpha}\frac{\partial^2\varepsilon_{\boldsymbol{k}}}{\partial k_i\partial k_j}n_{\boldsymbol{k}\alpha}. \quad (7)$$

In the case of a simple cubic or square lattice and the nearest-neighbor tight-binding dispersion relation, $\mathrm{Tr}\,K$ is proportional to the band energy (kinetic energy), $\Sigma\varepsilon_{\boldsymbol{k}}n_{\boldsymbol{k}\sigma}$, per unit cell. For this reason, K is also called the effective kinetic energy. Further, $\Pi_{ij}(\boldsymbol{q},\omega)$ in Eq. (6) is the retarded correlation function of the paramagnetic-current-density operator

$$\Pi_{ij}(\boldsymbol{q},\omega)=\frac{i}{\hbar}\int_{-\infty}^{\infty}dte^{i\omega t}\langle[j_i(\boldsymbol{q},t),j_j(-\boldsymbol{q},0)]\rangle\theta(t). \quad (8)$$

In the lowest order approximation, the correlator corresponds to a simple bubble diagram containing two independent quasiparticle lines. In the limit of small $\boldsymbol{q}$, its Matsubara counterpart can be written as

$$\Pi_{ij}(\boldsymbol{q},i\hbar\nu)=-\frac{e^2}{\hbar^2}\frac{1}{V\beta}\sum_{\boldsymbol{k},iE}\frac{\partial\varepsilon}{\partial k_i}\frac{\partial\varepsilon}{\partial k_j}\times\mathrm{Tr}[\mathcal{G}(\boldsymbol{k}+\boldsymbol{q},iE+i\hbar\nu)\mathcal{G}(\boldsymbol{k},iE)]. \quad (9)$$

This is the approximation mentioned in the Introduction, which is not gauge invariant and may lead to a violation of the sum rule (1).

A general field theoretical method to overcome the problem of gauge invariance was constructed by Nambu[19] in the context of the BCS theory. In the present context, it leads to the replacement of formula (9) with

$$\Pi_{ij}(\boldsymbol{q},i\hbar\nu)=-\frac{e^2}{\hbar^2}\frac{1}{V\beta}\sum_{\boldsymbol{k},iE}\frac{\partial\varepsilon}{\partial k_i}\times\mathrm{Tr}[\mathcal{G}(\boldsymbol{k}+\boldsymbol{q},iE+i\hbar\nu)\Gamma_j(\boldsymbol{k},iE,\boldsymbol{q},i\hbar\nu)\mathcal{G}(\boldsymbol{k},iE)]. \quad (10)$$

The bare vertex $\Gamma_j=(\partial\varepsilon/\partial k_j)\tau_0$ has been replaced with a renormalized one, $\Gamma_j(\boldsymbol{k},iE,\boldsymbol{q},i\hbar\nu)$ (2×2 matrix). For the theory to be gauge invariant, the renormalization of the vertex representing the coupling of the quasiparticles to the electromagnetic field has to be consistent with the renormalization of the quasiparticles by the interaction. It is known that Γ has to obey the generalized Ward identity, which is, in fact, a reformulated charge conservation law.[20] Within the simple Eliashberg theory, where the self-energy is $\boldsymbol{k}$ independent, this identity is satisfied already by the bare vertex. The minimal vertex satisfying the generalized Ward identity in

TABLE I. Values of the parameters used in the computations. Lattice parameters are denoted by a and d, t and t' are the parameters of the dispersion relation, n is the number of electrons per unit cell, and the meaning of the parameters ω_0, Γ, ξ, ω_C, Γ_C, and ξ_C specifying the spin susceptibility is explained in Ref. 6. For the normal state, we take $\Gamma=0.070$ eV and $\xi=1.57a$. The value of the input amplitude Δ_0 of Δ_k used within the hybrid approach was adjusted to yield the same amplitude of the resulting gap Δ as the self consistent approach. In the computations of Sec. III B, the values in the brackets have been used; the spectra shown in the Figs. 3–6 have been obtained with $g=3$ eV.

a (Å)	d (Å)	t (eV)	t' (eV)	n	g (eV)	$\hbar\omega_0$ (eV)	Γ (eV)	ξ (a)	$\hbar\omega_C$ (eV)	Γ_C (eV)	ξ_C (a)	b_M	b_C
3.828	11.650	0.250 (0.350)	−0.100	0.76(0.82)	2.0(2.0/3.0)	0.040	0.010	2.35	0.400	1.000	0.52	1	4

the present case of the self-energy given by Eq. (5) is the solution to the Bethe-Salpeter equation

$$\Gamma_j(\boldsymbol{k},iE,\boldsymbol{q},i\hbar\nu) = \frac{\partial\varepsilon}{\partial k_j}\tau_0 + \frac{g^2}{N\beta}\sum_{\boldsymbol{k}',iE'}\chi_{SF}(\boldsymbol{k}-\boldsymbol{k}',iE-iE') \times \mathcal{G}(\boldsymbol{k}'+\boldsymbol{q},iE'+i\hbar\nu)\Gamma_j(\boldsymbol{k}',iE',\boldsymbol{q},i\hbar\nu) \times \mathcal{G}(\boldsymbol{k}',iE'). \quad (11)$$

The second term on the right hand side of the equation is the VC. The correlator resulting from this gauge-invariant approach corresponds to the sum of all ladder diagrams, where noncrossing SF lines connecting the two quasiparticle lines are inserted into the conductivity bubble.

Formally, the hybrid approach can be made gauge invariant as well by using a somewhat simpler form of the renormalized vertex. The results, however, are qualitatively different from those of the self-consistent approach.

The input quantities of the theory are the dispersion relation ε_k, the chemical potential (or the electron density), the spin susceptibility χ_{SF}, and the coupling constant g. We have used the second nearest-neighbor tight-binding dispersion relation and the model spin susceptibility of the same form as in Ref. 6, containing the resonance mode and a continuum with dimensionless spectral weights of $0.01b_M$ and $0.01b_C$, respectively. The values of all input parameters are given in Table I. They are the same as in Ref. 6, except for g (1.52 eV in Ref. 6). The present value of g of 2 eV yields $T_c=64$ K and $\Delta=20$ meV (Δ is the amplitude of the gap). In the computations of Sec. III B, slightly different values of t, n, and g have been used; in Table I, they are given in parentheses.[21] For $g=2$ eV ($g=3$ eV), we obtain $T_c=77$ K and $\Delta=22$ meV ($T_c=89$ K and $\Delta=27$ meV).

Note that the present formulation assumes a single band only. In order to compare our results with experimental data on bilayer cuprates, we multiply the conductivity and related quantities (like K) by a factor $N_{\mathrm{pl}}=2$ reflecting the two planes in the unit cell. To address this issue carefully, we have also performed calculations with a model containing two bands—bonding and antibonding. The spin susceptibility was redistributed between the odd and even channels, the resonant mode being active in the odd channel.[22] The single-particle part of our computations is similar to that of Ref. 23. We have neglected the VC for simplicity. The results indicate that for reasonable values of the intrabilayer hopping matrix elements (of the order of 100 meV), the band splitting has a negligible effect on the in-plane conductivity, changing only the relative contributions of the bonding and antibonding bands to the resulting spectra.

The iterative solution of the self-energy equation (5) and especially of the Bethe-Salpeter equation (11) involves many convolutions both in Matsubara frequencies and in $\boldsymbol{k}$ space. Together with the requirement of high accuracy data for the subsequent analytical continuation to the real axis, this leads to a computationally very demanding task. We have performed the convolutions using the fast Fourier transform algorithm, taking the full advantage of the symmetries of Σ and Γ. Typically, we have used a grid of 96×96 points in the Brillouin zone and a cutoff of 10 eV (approximately 3.5 times the bandwidth) to limit the number of Matsubara frequencies. We have checked, by varying the density of the grid and the cutoff, that these values are sufficient. The analytical continuations to the real axis were performed using the standard method of Padé approximants.[24]

III. RESULTS AND DISCUSSION

A. Role of self-consistency

Here, we compare the conductivity spectra computed using the (non-self-consistent) hybrid approach with those of the self-consistent Eliashberg theory. Figure 1 shows the spectra of σ_1 (a) for the NS at $T=100$ K and (b) for the SCS at $T=20$ K. For the NS, the conductivity profiles are quite featureless. The dc value of the hybrid approach is by about 30% smaller. This is because the hybrid approach, which is—only for the NS—equivalent to the first iteration of Eq. (5), overestimates the magnitude of the quasiparticle self-energy.

Next we discuss the spectra for the SCS. They display an increase of σ_1 starting at low frequencies, which becomes steeper around $\hbar\omega_0+\Delta$ as discussed in Ref. 6. The character of the maximum following the onset, however, depends on the level of theory used. For the hybrid approach, the conductivity exhibits a very broad maximum, whereas the self-consistent approach yields a relatively sharp maximum near 800 cm^{-1}, consistent with experimental data.[25–27] The origin of this difference can be traced back to that of the quasiparticle spectral functions using the method presented in Ref. 6. It is based on the formula valid for the NS ($\boldsymbol{q}=0$),

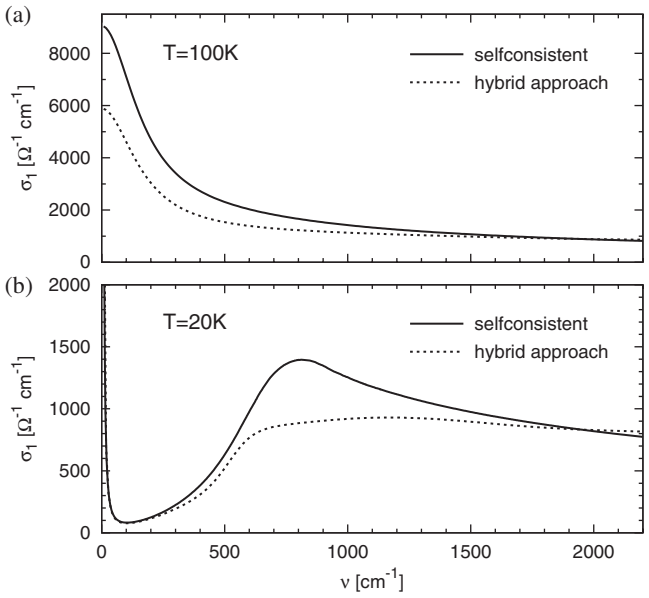

FIG. 1. Real part of the optical conductivity as obtained by using the self-consistent approach (solid lines) and the hybrid approach (dashed lines) for the normal state at $T=100$ K and for the superconducting state at $T=20$ K.

$$\sigma_1(\omega) \propto \frac{1}{\omega}\sum_{\boldsymbol{k}} \frac{1}{\hbar}\frac{\partial \varepsilon}{\partial k_i}\frac{1}{\hbar}\frac{\partial \varepsilon}{\partial k_j} \times \int A(\boldsymbol{k},E)A(\boldsymbol{k},E+\hbar\omega)[n_F(E)-n_F(E+\hbar\omega)]dE, \tag{12}$$

where $A(\boldsymbol{k},E)$ is the spectral function and n_F the Fermi function, and a similar formula involving the matrix spectral function valid for the SCS. These formulas allow one to understand the structures in the spectra of σ_1 in terms of "transitions" between various components of A. It has been shown in Refs. 3 and 6 that the onset of σ_1 in the SCS including the maximum is determined by transitions between the quasiparticle peaks and the incoherent parts of A. The spectral functions for selected $\boldsymbol{k}$ points are presented in Fig. 2. A detailed discussion of the spectral structures obtained at the hybrid level can be found in Ref. 6. Here, we concentrate on the comparison between the results of the self-consistent and the hybrid approach. The positions of the quasiparticle peaks Q and Q' are identical, which has been achieved by tuning the input BSC gap of the hybrid approach. The positions of the minima closest to the quasiparticle peaks are not much affected by self-consistency, thus giving a justification for using the hybrid approach to explain the low-energy dispersion anomalies.[18,23] The maxima P_1 and P_1' of the incoherent part in the self-consistent case are located closer to the quasiparticle peaks and are considerably sharper. This causes the steeper onset and the sharper maximum of σ_1. It can be seen that this maximum simply reflects the maxima of the incoherent part of A—P_1 and P_1'.

B. Vertex corrections

In this section, we focus on the central topic of the paper of how the model spectra change when the VC are included.

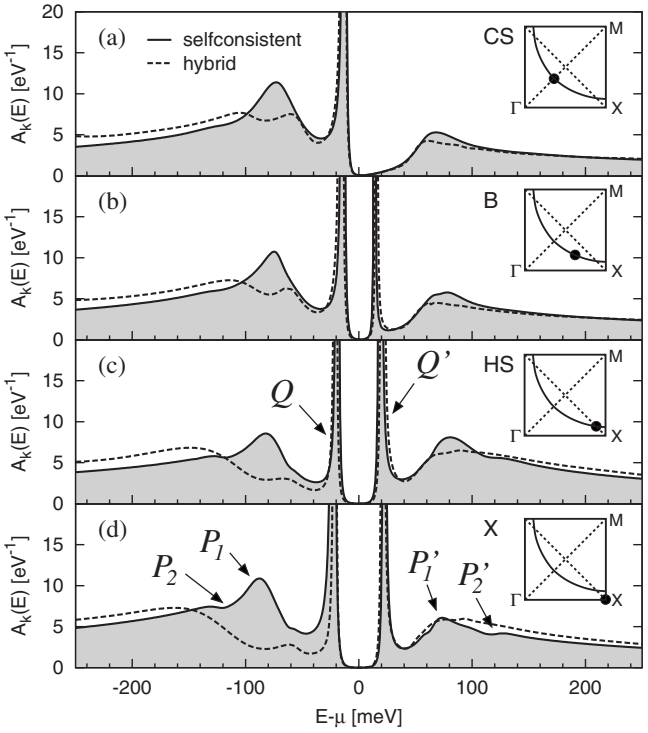

FIG. 2. Quasiparticle spectral functions for selected $\boldsymbol{k}$ points defined in Ref. 6 and shown in the insets as obtained by using the self-consistent approach (solid lines) and the hybrid approach (dashed lines) for the superconducting state at $T=20$ K. Our notation of spectral structures is introduced in (c) and (d).

Figure 3 shows the optical conductivity and three related quantities: the inverse scattering rate $[1/\tau](\omega)$ and the mass enhancement factor $[m^*/m](\omega)$, which are defined by the extended-Drude-model formula

$$\sigma(\omega) = \frac{\epsilon_0\omega_{\mathrm{pl}}^2}{[1/\tau](\omega) - i\omega[m^*/m](\omega)}, \tag{13}$$

where ω_{pl} is the plasma frequency and $W(\omega) = (2\pi)^{-1}d^2[\omega/\tau(\omega)]/d\omega^2$. For the NS of a weakly coupled isotropic electron-phonon system, the function $W(\omega)$ is approximately equal to the electron-phonon spectral density.[28,29] The solid line and the dashed line correspond to the SCS at $T=20$ K; the dashed-dotted line and the dotted line to the NS at $T=100$ K. The solid and the dashed-dotted lines (the dashed line and the dotted line) correspond to the self-consistent computation with (without) the VC. The values of the dc conductivity σ_{dc}, the effective kinetic energy K (multiplied by d to obtain the dimension of energy), the spectral weight at finite frequencies I_f, and that of the condensate I_c are given in Table II. The values of I_f and I_c have been multiplied by $2\hbar^2 d/\pi e^2$ to allow a direct comparison with those of Kd.

We begin our discussion with the NS. It can be seen in Table II that in the absence of VC, the sum rule $I_f \sim K$ (1) is not fulfilled. It means that the conductivity possesses an unphysical singular component, with the spectral weight I_c determined by Eq. (4). The values of I_c of about 3% (about 5%)

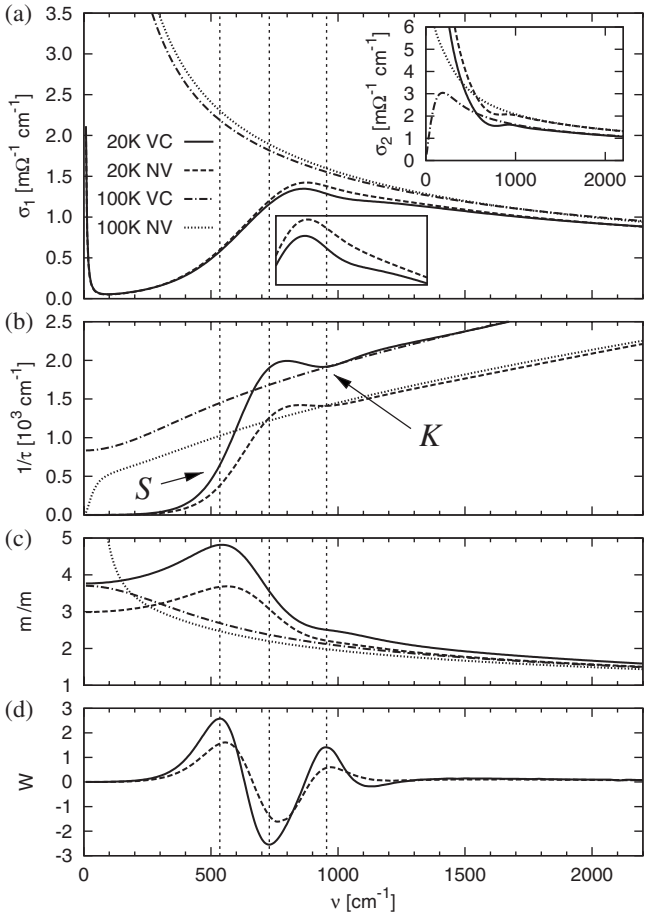

FIG. 3. The spectra of the optical conductivity, the inverse scattering rate, the mass enhancement factor, and the function W calculated with the vertex corrections neglected (NV) and with the vertex corrections included (VC) for the set of input parameters leading to realistic values of T_c and Δ. The insets of (a) show the vertically zoomed area near the conductivity maximum and the spectra of σ_2. In (d), only the superconducting state spectra are shown. The vertical dashed lines are drawn to guide the eye. A notation of spectral structures is introduced in (b).

of $-K$ for $g=2$ eV ($g=3$ eV) are small but significant. The unphysical component manifests itself also in the spectra of related quantities—see the spectra of σ_2 in the inset of Fig. 3(a), the drop of $1/\tau$ at low frequencies [Fig. 3(b)], and the corresponding divergence of m^*/m [Fig. 3(c)]. With the VC included, the sum rule is satisfied. The spectral-weight increase due to the VC $[\Delta I_f(\mathrm{VC})]$ is equal to I_c (within the numerical error related to discrete $\boldsymbol{k}$ sampling). Based on the relatively small values of I_c, the changes of the spectra due to the VC can be expected to be small. Indeed, only a slight decrease of σ_1 in the FIR can be observed in Fig. 3. The dc conductivity also decreases (see Table II), which is consistent with the results of Monthoux and Pines.[11] This trend, however, is not universal, as will be discussed in Sec. III B 1.

In the SCS, the VC increases I_f, which leads to a reduction of I_c (see Table II). This effect is explored in detail in Sec. III B 2. The real part of the conductivity is affected mainly near the maximum, around 800 cm^{-1}: the VC make it slightly sharper. The changes are further amplified in the spectra of related quantities $1/\tau$ and W, to be discussed in Sec. III B 3.

1. Spectral weight transfer from far infrared to midinfrared

Figure 3(a) shows a decrease of σ_1 in FIR with the incorporation of the VC which seems to be inconsistent with the increase of the finite-frequency spectral weight I_f. A resolution of this apparent controversy is provided by Fig. 4, which shows the contribution $\Delta\sigma_1(\mathrm{VC})$ of the VC to σ_1 in a wide spectral range. It can be seen that $\Delta\sigma_1(\mathrm{VC})$ is negative for $\omega<2000$ cm^{-1}, but positive for $\omega>2000$ cm^{-1}. The magnitude of the contribution of the latter spectral range to I_f is larger than that of the former, which leads to the total increase of I_f, both for the NS and for the SCS. For the SCS, the magnitude of $\Delta\sigma_1(\mathrm{VC})$ becomes small as the frequency approaches zero. This is due to the vanishing real part of conductivity in this limit. Figure 4 further demonstrates that the maximum of $\Delta\sigma_1(\mathrm{VC})$ shifts toward higher frequencies and becomes broader with increasing weight of the spin fluctuation continuum.

In order to explain the behavior displayed in Fig. 4, we use an extension of formula (12) that applies to the theory involving the VC. In the generalized formula, which has been obtained by manipulations starting from Eq. (10), the integral on the right hand side of Eq. (12) is replaced with a more general convolution of the spectral functions of the form $\int dE' \int dE'' A(\boldsymbol{k},E')A(\boldsymbol{k},E'')\Xi(E',E'',\hbar\omega)$, with the Matsubara counterpart of the convolution kernel given by

$$\Xi(E',E'',i\hbar\nu)=\frac{1}{\hbar\beta}\,\mathrm{Im}\sum_{iE}\frac{\Gamma(\boldsymbol{k},iE,i\hbar\nu)}{(iE+i\hbar\nu-E')(iE-E'')}. \tag{14}$$

If we use the bare vertex $\Gamma=\partial\varepsilon/\partial k$, we arrive at the relation $\Xi\propto\delta(E''+\hbar\omega-E')[n_F(E'')-n_F(E''+\hbar\omega)]$ which, after performing one of the integrations in the convolution, provides exactly formula (12). In contrast, any kernel Ξ corresponding to a frequency dependent renormalized vertex will be broader than the delta function and will result in a broadening of the conductivity profile.

The effect of the VC on the conductivity can be vaguely viewed as consisting of two ingredients: (a) the increase of the overall spectral weight I_f and (b) the broadening of the conductivity profile, which causes a transfer of spectral weight toward higher frequencies. The point (b) accounts for the trends shown in Fig. 4. The change of the dc conductivity is determined by a competition of (a) and (b). For our choice of the input parameters, the VC reduces the dc conductivity, in some cases; however, where $\Delta I_f(\mathrm{VC})$ is large, an increase of σ_{dc} may occur. Some examples can be found in Ref. 14.

The spectral-weight redistribution of Fig. 4 is similar to but considerably smaller than the one that could be expected based on the arguments by Millis *et al.*[10] Note, however, that the discrepancy between the value of the quasiparticle velocity along the Brillouin zone diagonal resulting from the present computations of 1.1 eV Å for $g=2$ eV (0.75 eV Å for $g=3$ eV) and the experimental value for YBCO of about 1.6 eV Å (Ref. 30) is not as dramatic as in Ref. 10.

TABLE II. Values of the effective kinetic energy K, the spectral weight at finite frequencies I_f, and the spectral weight of the singular component (condensate) I_c computed without vertex corrections (NV) and with the vertex corrections included (VC). The data are presented for two values of the coupling constant g; for the superconducting state at $T=20$ K and for the normal state at $T=100$ K. For the normal state, the values of the dc conductivity are also given.

	$g=2$ eV, $T_c=77$ K, $\Delta_X=22$ meV (20 K)				
	$T=20$ K, $Kd=-0.44688$ eV		$T=100$ K, $Kd=-0.44653$ eV		
	I_f (eV)	I_c (eV)	I_f (eV)	$I_c/\lvert K\rvert$ (%)	σ_{dc} (Ω^{-1} cm^{-1})
NV	0.27079	0.17609	0.43205	3.2	1.62×10^4
VC	0.29752	0.14936	0.44624	0.1	1.41×10^4
	$g=3$ eV, $T_c=89$ K, $\Delta_X=27$ meV (20 K)				
	$T=20$ K, $Kd=-0.40741$ eV		$T=100$ K, $Kd=-0.40699$ eV		
	I_f (eV)	I_c (eV)	I_f (eV)	$I_c/\lvert K\rvert$ (%)	σ_{dc} (Ω^{-1} cm^{-1})
NV	0.28871	0.11870	0.38580	5.2	8.0×10^3
VC	0.31312	0.09429	0.40699	0.0	7.5×10^3

2. *Effect of the vertex corrections on the spectral weight of the condensate*

We have already noted that the VC significantly increases the values of I_f and reduces those of I_c.

This is further documented in Fig. 5, which shows I_f and I_c as functions of the coupling constant g. For values of g^2 of 4–10 eV^2, leading to reasonable values of T_c and Δ, the magnitude of ΔI_f(VC) is about 6% of that of K. It can be seen in Fig. 5(b) that the corresponding change in the condensate weight I_c is up to 20%. At low values of g, ΔI_f(VC) scales with g^2. This can be easily interpreted by considering the diagram series for the correlator (10). The contribution of a diagram with N spin-fluctuation lines connecting the quasiparticle lines in the bubble is proportional to g^{2N}. In the limit of small g, only the lowest-order diagrams ($N=0$ and $N=1$) survive, leading to the observed behavior.

The temperature dependence of the effective kinetic energy K and the band energy $KE=\Sigma\epsilon_k n_{k\sigma}$ obtained within the Eliashberg theory with SF was already discussed in Ref. 31. Our approach yields a similar behavior of the two quantities. The resulting value of $K(\mathrm{NS}, T=20\ \mathrm{K})-K(\mathrm{SCS}, T=20\ \mathrm{K})$ is also similar to that obtained by Cásek *et al.*[6] using the hybrid

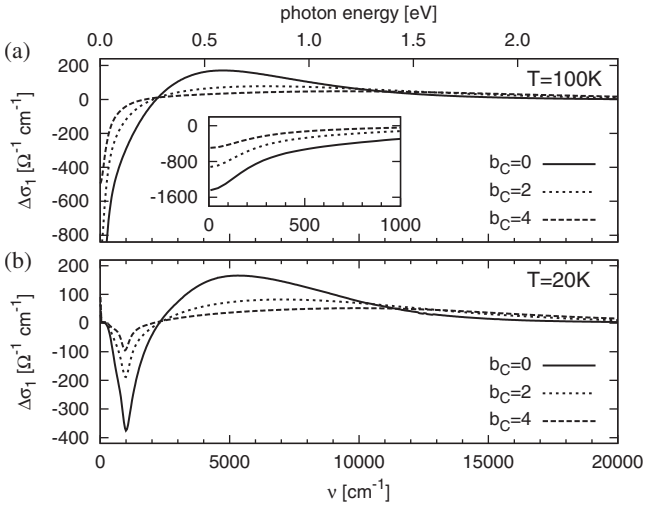

FIG. 4. (a) Contribution of the VC to the real part of the normal state conductivity at $T=100$ K for various values of the relative spin-continuum weight b_C. The low-energy parts of the spectra are shown in the inset. (b) The same for the superconducting state at $T=20$ K.

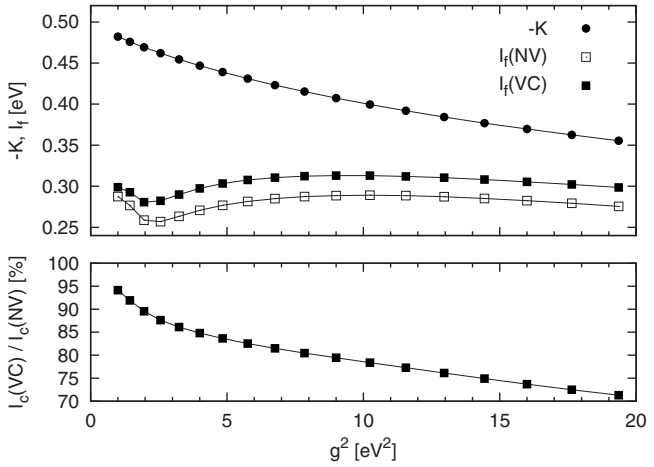

FIG. 5. (a) The coupling-constant dependence of the effective kinetic energy and of the intraband spectral weight obtained with the vertex corrections neglected (NV) and with the vertex corrections included (VC). (b) The coupling-constant dependence of the ratio of the condensate weight obtained with the vertex corrections included to that obtained using the vertex corrections neglected.

approach. The analysis published in Ref. 6, however, cannot be easily extended to the present fully self-consistent theory. The contribution $\Delta I_f(\mathrm{VC})$ of the VC to I_f is only weakly temperature dependent above T_c. Below T_c, $\Delta I_f(\mathrm{VC})$ slightly decreases, exhibits a minimum, and then increases. The low temperature value is somewhat higher than that of the NS.

3. Spectral structures of $[1/\tau](\omega)$ and $W(\omega)$ for the superconducting state

Having discussed the global trends of the spectral changes due to the VC, we concentrate here on pronounced features in the spectra of $1/\tau$ and W. The SCS spectra of $1/\tau$ shown in Fig. 3 exhibit the famous onset starting around the frequency of the resonance mode ω_0, becoming steeper around 500 cm^{-1} (this feature is labeled as S), and reaching a sharp maximum around 800 cm^{-1}. Surprisingly, the maximum is followed by a kink labeled as K. Note that the spectra are fairly similar to the experimental ones of optimally doped materials.[25–27] All these features appear already in the spectra of σ_1; however, they are more pronounced in $1/\tau$. The function W is approximately proportional to the second derivative of $1/\tau$, and can thus be expected to possess two maxima corresponding to the structures S and K and a minimum close to the maximum of $1/\tau$. This is indeed the case, as shown in Fig. 3(d).

The origin of the feature S has been elucidated by Cásek *et al.*[6] It is due to the appearance above $\hbar\omega_0+\Delta$ of excitations of the nodal region, consisting of a nodal quasiparticle, an antinodal quasiparticle, and the resonance mode. The arguments of Ref. 6, even though formulated at the level of the hybrid approach, remain to be valid also in the context of the present fully self-consistent theory. As noted for the first time by Carbotte *et al.*,[4] the energy of the relevant maximum in W is close to $\hbar\omega_0+\Delta$.

The sharp maximum of $1/\tau$ and the corresponding minimum of W can be shown to result from transitions $P_1 \rightarrow Q'$ and $Q \rightarrow P_1'$ (see Fig. 2). The energy of the structure is close to $\hbar\omega_0+2\Delta$, which can be understood using the arguments presented in Ref. 6. The presence of this characteristic energy scale in the optical spectra of the high-T_c cuprates has been for the first time predicted by Abanov *et al.*[5] In their work, the corresponding spectral structure is attributed to processes involving a Bogoljubov quasiparticle with energy Δ and a sharp onset of the incoherent part of $A(\boldsymbol{k},E)$ at $\Delta+\hbar\omega_0$.

The kink labeled as K can also be interpreted in terms of the quasiparticle spectral functions. Note that the maxima P_1 and P_1' in Fig. 2 that are connected to the maximum of σ_1 and the related structures in the spectra of $1/\tau$ and W are followed by shoulder features, labeled as P_2 and P_2', on their high-energy sides. They can be expected, based on Eq. (12), to manifest themselves also in the conductivity. Our detailed calculations show that (a) the shoulder features are indeed responsible for the kink K in $1/\tau$ and (b) they can be attributed to excited states involving two magnetic excitations. We recall that the maxima P_1 and P_1' correspond to excited states involving one Bogoljubov quasiparticle and just one magnetic excitation. The characteristic energy of the shoulder features is $2\hbar\omega_0+\Delta$ and that of the kink K (which can be associated with transitions $P_2 \rightarrow Q'$ and $Q \rightarrow P_2'$) is $2\hbar\omega_0+2\Delta$. Abanov *et al.*[5] also predicted a structure located at $2\hbar\omega_0+2\Delta$. Their interpretation, however, differs from ours. In their theory, the structure is due to transitions between negative- and positive-energy satellites (incoherent components) of A.

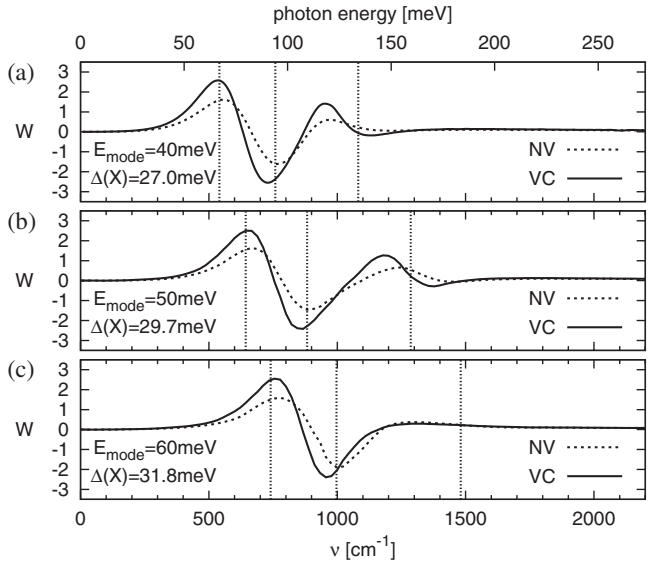

FIG. 6. The function W for the superconducting state at $T=20$ K obtained with the vertex corrections neglected (NV) and with the vertex corrections included (VC) for three values of the energy of the resonant mode in the spin susceptibility. The vertical lines are located at the characteristic energies of $\hbar\omega_0+\Delta$, $\hbar\omega_0+2\Delta$, and $2\hbar\omega_0+2\Delta$.

In order to check the proposed assignment of the spectral structures, we have studied the ω_0 dependence of $1/\tau$ and W. Figure 6 shows the spectra of W for three values of the energy of the magnetic mode. It can be seen that the first maximum and the minimum are located close to $\hbar\omega_0+\Delta$ and $\hbar\omega_0+2\Delta$, respectively, in agreement with the above considerations. The second maximum corresponding to the kink is, in the absence of VC, located somewhat below $2\hbar\omega_0+2\Delta$.

Finally, we address the role of the VC. They lead (a) to an increase in the amplitude of the structures of $1/\tau$ and W, which is due to the combined effect of the significant decrease of σ_2 [see the inset of Fig. 3(a)] and a sharpening of the features in σ_1, and (b) to a slight shift of the structures toward lower energies. The shift may be partially caused by a weak attractive interaction between the quasiparticles, leading to an excitonic effect.

IV. SUMMARY AND CONCLUSIONS

The changes of the infrared conductivity caused by the VCs are not dramatic, which provides a justification for earlier computations where these corrections were neglected. Some aspects of the changes, however, appear to be important.

(i) The normal state conductivity computed without the VC does not satisfy the restricted sum rule. The calculated

spectral weight at finite frequencies (I_f) is by a few percent lower than the value dictated by the sum rule. The incorporation of the VC leads to the increase of I_f, removing this discrepancy.

(ii) The increase of I_f is associated with a broadening of σ_1. The far-infrared conductivity (including the dc value) may decrease or increase depending on the magnitude of the change of I_f and the degree of the broadening; at high frequencies, the conductivity increases. For our values of the input parameters, σ_1 decreases (increases) below (above) about 2000 cm^{-1}.

(iii) The increase of I_f occurs also for the superconducting state. Since the sum of I_f and the spectral weight of the superconducting condensate remains constant, this implies a reduction of the latter. For relevant values of the input parameters, the weight of the condensate decreases by 15%–20%.

(iv) The VCs lead to an amplification of the characteristic features in the superconducting state spectra of the inverse scattering rate $1/\tau$, which have been used to support the spin-fluctuation scenario: the onset of $1/\tau$ around 500 cm^{-1} becomes steeper and the maximum around 800 cm^{-1} more pronounced.

In addition to studying the changes brought about by the VC, we have also investigated the role of self-consistency by comparing the results obtained using the self-consistent Eliashberg equations with those of the non-self-consistent hybrid approach (i.e., approximately, the first iteration of the equations). The main results are (a) the hybrid approach considerably overestimates the magnitude of the quasiparticle self-energy, which leads to lower values of the conductivity in the far infrared, and (b) some spectral features, in particular, the sharp maximum in the superconducting state spectra centered at about 800 cm^{-1} and the kink at about 1000 cm^{-1}, appear only at the self-consistent level. With the aid of the quasiparticle spectral function A, we attribute the kink to the onset of transitions involving incoherent satellites of A corresponding to states with doubly excited resonance mode.[32]

The computed spectra are in reasonable agreement with experimental data of optimally doped cuprates, including such details as the shape of the maximum in the inverse scattering rate. In addition, the theory allows one to interpret most of the features of the data in terms of Bogoljubov quasiparticles and magnetic excitations. In the superconducting state, a crucial role is played by the resonance mode. We are not aware of any comparable interpretation in terms of electron-phonon coupling.

ACKNOWLEDGMENTS

This work was supported by the Ministry of Education of Czech Republic (MSM0021622410). J.Ch. thanks B. Keimer and G. Khaliullin for their hospitality during a stay at MPI Stuttgart. We gratefully acknowledge helpful discussions with J. Humlíček, C. Bernhard, A.V. Boris, N.N. Kovaleva, and B. Keimer.

*chaloupka@physics.muni.cz

[1] S. M. Quinlan, P. J. Hirschfeld, and D. J. Scalapino, Phys. Rev. B **53**, 8575 (1996).
[2] E. Schachinger, J. P. Carbotte, and F. Marsiglio, Phys. Rev. B **56**, 2738 (1997).
[3] D. Munzar, C. Bernhard, and M. Cardona, Physica C **312**, 121 (1999).
[4] J. P. Carbotte, E. Schachinger, and D. N. Basov, Nature (London) **401**, 354 (1999).
[5] A. Abanov, A. V. Chubukov, and J. Schmalian, Phys. Rev. B **63**, 180510(R) (2001).
[6] P. Cásek, C. Bernhard, J. Humlíček, and D. Munzar, Phys. Rev. B **72**, 134526 (2005).
[7] J. Hwang, T. Timusk, E. Schachinger, and J. P. Carbotte, Phys. Rev. B **75**, 144508 (2007).
[8] P. Nozieres and D. Pines, *The Theory of Quantum Liquids* (Perseus, Cambridge, MA, 1999).
[9] A. J. Millis and H. D. Drew, Phys. Rev. B **67**, 214517 (2003).
[10] A. J. Millis, A. Zimmers, R. P. S. M. Lobo, N. Bontemps, and C. C. Homes, Phys. Rev. B **72**, 224517 (2005).
[11] P. Monthoux and D. Pines, Phys. Rev. B **49**, 4261 (1994).
[12] D. Manske, *Theory of Unconventional Superconductors* (Springer-Verlag, Berlin, 2004).
[13] H. Kontani, J. Phys. Soc. Jpn. **75**, 013703 (2006).
[14] H. Kontani, J. Phys. Soc. Jpn. **76**, 074707 (2007).
[15] L. Benfatto, S. G. Sharapov, N. Andrenacci, and H. Beck, Phys. Rev. B **71**, 104511 (2005).
[16] D. N. Aristov and R. Zeyher, Phys. Rev. B **72**, 115118 (2005).
[17] P. Monthoux and D. Pines, Phys. Rev. B **47**, 6069 (1993).
[18] M. Eschrig and M. R. Norman, Phys. Rev. B **67**, 144503 (2003).
[19] Y. Nambu, Phys. Rev. **117**, 648 (1960).
[20] J. R. Schrieffer, *Theory of Superconductivity* (Addison-Wesley, Reading, MA, 1988).
[21] The values of t and t' are close to the LDA results published in O. K. Andersen, A. I. Liechtenstein, O. Jepsen, and F. Paulsen, J. Phys. Chem. Solids **56**, 1573 (1995).
[22] H. F. Fong, P. Bourges, Y. Sidis, L. P. Regnault, J. Bossy, A. Ivanov, D. L. Milius, I. A. Aksay, and B. Keimer, Phys. Rev. B **61**, 14773 (2000).
[23] M. Eschrig and M. R. Norman, Phys. Rev. Lett. **89**, 277005 (2002).
[24] H. J. Vidberg and J. W. Serene, J. Low Temp. Phys. **29**, 179 (1977).
[25] A. V. Boris, N. N. Kovaleva, O. V. Dolgov, T. Holden, C. T. Lin, B. Keimer, and C. Bernhard, Science **304**, 708 (2004).
[26] D. van der Marel, H. J. A. Molegraaf, J. Zaanen, Z. Nussinov, F. Carbone, A. Damascelli, H. Eisaki, M. Greven, P. H. Kes, and M. Li, Nature (London) **425**, 271 (2003).
[27] J. Hwang, T. Timusk, and D. G. Gu, Nature (London) **427**, 714 (2004).
[28] F. Marsiglio, T. Startseva, and J. P. Carbotte, Phys. Lett. A **245**, 172 (1998).
[29] S. V. Schulga, in *Material Science, Fundamental Properties and Future Electronic Applications of High-Tc Superconductors*, ed-

ited by S. L. Drechsler and T. Mischonov (Kluwer Academic, Dordrecht, 2001), pp. 323–360.

[30] S. V. Borisenko, A. A. Kordyuk, V. Zabolotnyy, J. Geck, D. Inosov, A. Koitzsch, J. Fink, M. Knupfer, B. Büchner, V. Hinkov, C. T. Lin, B. Keimer, T. Wolf, S. G. Chiuzbăian, L. Patthey, and R. Follath, Phys. Rev. Lett. **96**, 117004 (2006).

[31] E. Schachinger and J. P. Carbotte, Phys. Rev. B **72**, 014535 (2005).

[32] Note that multiple excitations of the resonance mode are not included at the hybrid level.